Continuous $CaO/Ca(OH)_2$ fluidized bed reactor for energy storage: first experimental results and reactor model validation

Sylvie Rougé*[a], Yolanda A. Criado[b], Olivier Soriano[a] J. Carlos Abanades[b]

[a]Commissariat à l'Energie Atomique et aux Energies Alternatives, LITEN- CEA, 17 rue des martyrs, 38054, Grenoble Cedex 09, France

[b]CSIC-INCAR, C/ Francisco Pintado Fe, 26, 33011, Oviedo. Spain.

*Corresponding Author: Tel: +33 4 38 78 68 84; Fax: +33 4 38 78 54 35, e-mail: sylvie.rouge@cea.fr

Abstract

Novel thermochemical energy storage systems that employ fluidized beds of $CaO/Ca(OH)_2$ for hydration/dehydration reactions are under development because of the inherent advantages of the low cost of the materials and their relatively high temperature operation windows (450ºC-550ºC). We report in this work the results of the first steady state experiments conducted in a new pilot plant designed to test the concept under realistic reactor conditions. The pilot has a fluidized bed reactor with an internal diameter of 0.108 m and a height of 780 mm fed continuously with gas and solids as well as heat exchangers to supply/extract the required reaction heat. The experimental results during dynamic and steady state periods were fitted to a KL reactor bubbling bed model, using kinetic parameters from thermogravimetric studies and a single crossflow factor. The resulting continuous reactor model will serve as useful tool for the continued scaling up of this technology.

Introduction

The widespread deployment of renewable energy sources is essential to reduce greenhouse emissions and to mitigate climate change[1, 2]. In particular, the production of electricity from concentrated solar power (CSP) installations has increased considerably in the last decade, from a total installed capacity of 0.4 GW in 2006 to 4.6 GW at the present time[3]. In order to achieve more reliable energy production and dispatchability in CSP plants, the use of large scale heat storage systems is essential to allow electricity production to keep up with demand[4-7].

Thermochemical energy storage systems (TCS) are considered a good option[5, 8-12] because of their theoretically higher energy storage density and capacities, higher working temperatures and smaller heat losses when compared to standard thermal energy storage systems based on sensible and latent heat[10]. Despite these theoretical advantages, TCS systems have only been studied at a conceptual level and are far from having reached industrial maturity. Several chemical reaction couples are being investigated for their use as TCS in CSP plants[5, 8, 11, 12] with some of the basic process schemes dating back to the late 70's[13-15]. Of the different reaction schemes, the hydration/dehydration of $CaO/Ca(OH)_2$ has been presented as a suitable candidate for CSP plants because of the range of temperatures of these reactions (400-600ºC), which is similar to the temperature levels of the steam cycles in current CSP plants. In addition, the reaction enthalpy is high (104 kJ/mol), the reaction rates are fast and highly reversible[16] and the material is low cost, abundant and non-toxic[8].

The basic conceptual scheme of the $CaO/Ca(OH)_2$ chemical loop[15] (as shown in Figure 1) consists of an initial hydration reaction (discharge step), where heat is released (Q_{OUT}) at a constant high temperature from the exothermic reaction between CaO and $H_2O_{(v)}$. The $Ca(OH)_2$ formed during the discharge step is stored for use during the

charge step (dehydration reaction). The CaO is regenerated during dehydration by providing the heat required for the endothermic reaction to take place (Q_{IN}). Several schemes for integrating the charge and discharge steps of the TCS system in a CSP plant have been studied within the FP7 European Project StoRRe (http://www.storre-project.eu/), of which this study forms a part. Some of the proposed integration schemes are based on direct heat transfer during the charge step (i.e. by dehydrating the solids in the solar field, as proposed[17, 18] for the calcination of $CaCO_3$). It is also possible to conceive of process schemes where indirect heat transfer takes place during the charge step by using heat transfer fluids such as high temperature molten salts, liquid metals[19], supercritical CO_2 [20] or dense particle suspensions as proposed by Flamant et al.[21-23] to transfer energy from the solar receiver. Integration schemes for the discharge step, designed to exploit the constant temperature maintained by the hydration reaction in the power block or steam cycle of the CSP plant, have also been studied. However, the present work is focused only on reactor performance, it being assumed that a power input supplies the heat required for the dehydration reaction, while exothermic reaction heat is transferred to the power block during the discharge step.

The reactor(s) required to carry out the fast gas-solid hydration and dehydration reactions of a $CaO/Ca(OH)_2$ TCS system need(s) to be designed in such way as to minimize heat and mass transfer limitations and to be scalable up to the 100 MW_{th} range, which is the capacity of state-of-the-art CSP thermal power technology. Fluidized bed (FB) reactors have been proposed as a suitable reactor choice for these reactions[24] because they have reasonably high heat transfer coefficients that are necessary to extract/supply the required exothermic/endothermic heat[25]. Other authors have proposed using fixed or moving beds[26-31] as reference reactors for the $CaO/Ca(OH)_2$ hydration/dehydration reactions. However, the low heat transfer

coefficients and the large pressure drops and/or the large cross-sections required to feed/extract the reactant gas are important challenges for fixed bed systems for this application.

In previous works[32, 33], encouraging results were obtained from the study of hydration/dehydration reactions in a batch bubbling fluidized bed reactor. For the present work a new experimental facility has been designed and built at CEA-Grenoble to prove the viability of the concept using a continuous feed of solid and gas reactants. The reactor type in this new facility is a bubbling fluidized bed that employs external and submerged heat exchangers to maintain the temperature in the reactor constant as heat generated or consumed during each hydration/dehydration reaction is removed or supplied. The reactors are operated under realistic operation conditions (i.e. high fluidization velocities, temperatures above 400ºC and high partial pressures of $H_2O_{(v)}$). The first experimental results (obtained after hours of operation in steady state mode) are compared with a standard KL bubbling reactor.

Experimental section

Experimental setup

The experimental facility is shown in Figure 2. The reactor consists of a cylinder of 108 mm internal diameter and 780 mm height made of Inconel 600 alloy that makes it possible to operate at temperatures up to 800ºC at the walls and at a maximum pressure of 150 kPa. Several electric heaters located along the reactor walls are able to provide a maximum of 20 kW to the reactor (see the main HX1-4 and the solid preheaters HX_{solids} in Figure 2) during the $Ca(OH)_2$ dehydration step. During the hydration step, the heat generated by the exothermic reaction is removed by a submerged heat-exchanger, using air as heat transfer fluid (up to 60 Nm^3/h) to exchange up to 4 kW.

In this facility, both hydration and dehydration can be performed either under pure steam or under mixtures of steam and air, bed temperatures of up to 600ºC, fluidizing gas velocities of up to 2 m/s, solids flow rates of up to 20 kg/s using particles up to 1.5 mm in diameter. Two separate circuits provide air (up to 40 Nm^3/h) and/or $H_2O_{(v)}$ (up to 32 kg/h). Before entering the reactor section, the air stream is preheated up to 200ºC while liquid water is vaporized and then superheated up to 250ºC. The air/$H_2O_{(v)}$ mixture is further superheated up to the reaction temperature before entering the bed through a heated cone (HX1 in Figure 2). At the bottom of the bed, there is a gas distributor consisting of a plate in which 21 drilled screws of diameter 2 mm have been introduced to act as nozzles.

The temperature inside the bed is measured at four different levels using at each level three K-type thermocouples in different radial positions. At the reactor wall, the temperature is measured by two K-type thermocouples positioned near each heater. Pressure measurements are taken before the gas distributor, at four different levels in the reactor bed and after the filter.

To supply a continuous and steady flow of solids during several hours of operation, a feeding system consisting of two 80-liter hoppers, a cold regulating feeding screw and a warm transport screw connected to the lower part of the reactor, have been incorporated (see left-hand side of Figure 2). Two rotary valves prevent the mixture of gases from flowing towards the hoppers. The solids flowrate is measured by both the speed of rotation of the regulation screw and by the weight sensors in each hopper.

In order to extract the mixture of reacted solids and gases from the reactor section, a pneumatic line is employed using a constant flow of hot air at high velocity (20 m/s) as transport gas before the gas is separated from the solids by a high temperature filter (up to 200ºC). In order to reduce the temperature of the stream exiting the reactor (at

temperatures above 400ºC) the pneumatic line is cooled by natural convection by means of external fins located along the line. The solids, once separated from the gas, are delivered to the second hopper.

The conversion of the solids during the hydration and dehydration reactions is followed by a mass balance of the water mass flow rate (m_{H2O}) between the inlet and outlet of the reactor. As will be explained below, a heat balance can also be carried to the bed to measure the degree and intensity of the reactions at any point in time. The m_{H2O} at the exit of the reactor is measured by two capacitive hygrometers VAISALA and ROTRONIC respectively (see HYG2 and HYG3 in Figure 2) calibrated by taking into account the pressure and temperatures at their location. To control the overall conversion yield, samples of solids before and after testing can be extracted from the hoppers and tested in a laboratory oven. Continuous solids sampling from the reactor for solids conversion measurements during testing was not possible due to blockage problems in the solids sampling ports.

Experimental procedure

The following set of experimental conditions was chosen for this experimental facility: a reactor temperature of between 400-600ºC, an inlet gas velocity of between 0.2 and 1.5 m/s, a $H_2O_{(v)}$ fraction of between 0 and 1 and a solids flow rate of between 5 and 20 kg/s. In a typical test, the solids hopper 1 is filled with $CaO/Ca(OH)_2$ solids. The facility is then preheated and the air flowrates fixed to the desired experimental values. In the hydration tests under a certain inlet fraction of $H_2O_{(v)}$ ($v_{H2O,\ in}$), the steam generator is connected and the submerged heat exchanger circuit is switched on. Each experiment is carried out under a steady state of solid and gas feeding for a few hours (typically 3-5 h, depending on the solids flow) until the first hopper is empty and the second one is full.

At the end of each experiment, in order to start a new test (dehydration after a hydration and vice versa), the solids are transferred by gravity from the second to the first hopper.

Materials characterization

The lime provided for the continuous tests is a commercial grade 95%w CaO, supplied by Carmeuse, obtained by the calcination of $CaCO_3$ at 1000°C sieved to a particle size range of 200-800 μm. The CaO material was chemically and mechanically characterized elsewhere[32] by thermogravimetric analysis and by crushing strength measurements. The commercial material employed for the experimental campaign described in this work is suitable for use during a few cycles without generating a large fraction of fines at the expense of modest conversions and lower hydration rates. Other much more stable materials have been developed within the StoRRe project[34, 35] but cannot yet be manufactured at the scales required for the pilot (i.e. hundreds of kg).

Results and discussion

Results from a typical hydration and dehydration test

Examples of results obtained from typical hydration and dehydration reaction tests are shown in Figures 3 and 4 respectively, where some of the main variables measured during the test are plotted vs time. As can be seen, there is a good control of the solids (m_{Ca}) and gas flow rates (m_{air} and $m_{H2O,in}$) and the desired set points for these variables remain unchanged over several hours of testing. Furthermore, the bed temperature (T_{Bed}) remains reasonably constant during the steady state operation mode (from min 50 and min 2 onwards in Figures 3 and 4 at 400ºC and 540ºC respectively). No significant temperature profiles were observed within the bed, indicating a good mixing of the solids. The $H_2O_{(v)}$ outflow measurements recorded by the two hygrometers located at

the exit of the reactor show a good agreement between both hygrometers (see $m_{H2O,exit\ HYG2}$ and $m_{H2O,\ exit\ HYG\ 3}$ lines in Figures 3 and 4).

The hydration test in Figure 3 starts with an initial bed partially filled with material dehydrated from a previous test. During the first few minutes (from 0 to 50 min) no solids are fed in, whereas the air/$H_2O_{(v)}$ mixture is introduced into the bed (corresponding to a $v_{H2O,\ in}$=0.5 and a u_{in}=0.6 m/s). Under these circumstances, the dehydrated solids present in the bed behave as a batch reactor that consumes part of the inlet $H_2O_{(v)}$ until complete conversion of the active CaO present in the bed is achieved (min 15 in Figure 3). As expected, at that point the outflow of $H_2O_{(v)}$ measured by the hygrometers is in agreement with the inflow of $H_2O_{(v)}$. When the solids feeding system is switched on (min 50 in Figure 3), a significant drop in the outflow of $H_2O_{(v)}$ is recorded by both hygrometers until a constant value of ~ 2.4 kg/h is reached. When the infeed of solids is stopped and the reaction ends (min 315 in Figure 3) the $m_{H2O,\ exit}$ values measured by both hygrometers are in concordance with the $m_{H2O,\ in}$. During the steady state, the cooling power is set at a constant value (see "Cooling" line in Figure 3) and the bed temperature is regulated by the electric heaters HX2- 4 that also compensate for heat losses (maintained at values of around 0.3-0.7 kW for each heat exchanger throughout the experimental tests shown in Figure 3). Also, around 0.7 kW are used on the screw line in order to preheat the solids before entering the bed (see HX_{solids} in Figure 3). When the solids feeding starts, the heating power should be reduced sharply in order to compensate for the chemical heat but since a certain sensible heat must be provided at the same time to the solids entering the reactor (at a temperature lower than T_{Bed}), the decrease of the heating power is minor, as can be seen in Figure 3. The effective chemical heat produced during hydration is calculated by taking into account the heat power delivered to the bed by the different HX (both around the bed and on the

screw line) as well as the heat removed by the submerged heat exchanger, the sensible heat of the solids and the heat losses.

At the beginning of the dehydration test shown in Figure 4, the emptied bed is fed with pure air (equivalent to a gas velocity of u_{in}=0.65 m/s). When the feeding screw is turned on at min 1, a sharp increase in $H_2O_{(v)}$ flow is recorded at the exit of the reactor. This $H_2O_{(v)}$ production remains constant and stops sharply at the end of the solids feeding (min 220). During dehydration, the submerged heat exchanger is switched off (as it is not very efficient to use this device as a heating system, due to the temperature restrictions). As soon as the solids enter the bed, a sharp increase in the power delivered to the bed by the electric heaters is observed. This power is used to provide the heat for dehydration but also to heat the flow of solids coming into the bed (at a lower temperature than T_{Bed}) and to compensate for heat losses, and so the increase of power delivered to the bed cannot be directly related to the dehydration power. At the end of the test, the HX power decreases rapidly and is only used to compensate for heat losses. This value is also used to calibrate in-situ the system heat losses. It must be taken into account that the required power to heat the solids is around one order of magnitude higher than the heat losses (1.5-2 kW at 12 kg/h of solids vs. 0.4-0.7 kW at 400-550ºC), even when part of the solids preheating is done in the hot feeding screw line (see HX_{solids} lines in Figures 3 and 4).

A solid mass balance closure by measuring the change in solids conversion in samples of solids along testing was not possible because of problems with the solid sampling probes, as mentioned above. In some cases, it was possible to obtain samples from the solid hoppers after testing, showing a good agreement with the solids conversion calculated from the hygrometers measurements. An alternative check of the measurements in the gas phase can be obtained by applying a mass and heat balance

around the reactor boundaries. As previously mentioned, the reaction heat generated during the hydration reaction is removed from the bed by the submerged heat-exchanger using air as heat transfer fluid. Since the bed temperature is kept constant throughout the experiments thanks to electric heaters (HX2, HX3 and HX4 in Figure 3) that also compensate for heat losses and heat the solids, the excess heat generated by the hydration reaction can only be removed by the internal air heat-exchanger (this is equivalent to assume that the reactor operates in adiabatic conditions during the hydration step). Based on this assumption, it is possible to calculate the mass flow of $H_2O_{(v)}$ at the exit of the reactor from the heat balance, and compare it with the direct measurements recorded by the hygrometers. The experimental results in Figure 3 ($m_{H2O,\ exit\ Q}$ vs. $m_{H2O,\ exit\ HYG2}$ and $m_{H2O,\ exit\ HYG3}$ lines), show that there is a good agreement between the flow of $H_2O_{(v)}$ at the exit of the reactor calculated by the heat balance and that measured by the two hygrometers. Figure 5 represents the same comparison for three different hydration experiments with different inlet fractions of $H_2O_{(v)}$. The results suggest that it should be possible to follow the progress of the hydration reaction from the heat balance to the bed.

In contrast, during the dehydration reaction it is not possible to follow the progress of the reaction by applying a heat balance to the reactor. In this case, the heat input for dehydration does not come from the air-heat exchanger submerged in the reactor but from the external electric heaters (HX2, HX3 and HX4 signals in Figure 4). For reasons not fully understood, probably linked to the higher fluidizing velocities at the top of the bed and possible turbulence induced by the transport air in this region, the closure of the heat balance does not provide so far information of sufficient quality to derive the dehydration conversion (see, for example, Figure 4 where there are noticeable

differences in the flows of $H_2O_{(v)}$ at the exit of the reactor given by the hygrometers and by the heat balance).

Reactor modeling and comparison with first experimental results

The bubbling bed reactor model of Kunii-Levenspiel[25] has been adapted in this work for the hydration and dehydration reactions in the continuous pilot plant (see Figure 6) described in the previous sections. Since the first experiments were performed under fractions of $H_2O_{(v)}$ $\nu_{H2O}<1$, the reactor model must take into account the presence of an axial profile of ν_{H2O} in the bubbling phase (assumed to be free of solids). All the gas-solid reactions take place in the emulsion phase (assumed to be under minimum fluidization conditions). A certain gas exchange between the bubble and emulsion phases is also assumed (see right hand side of Figure 6). The axial profile of $H_2O_{(v)}$ is calculated by the model. However only the exit concentration of $H_2O_{(v)}$ can be compared with and validated against the experimental results.

The model equations described below refer to the hydration reaction only. They can be applied to the dehydration stages, simply by changing the sign of the $H_2O_{(v)}$ reacting flows and the notation. The model must be able to fit and interpret two different modes of reactor operations that can be observed in the experimental results: (i) operation modes in dynamic conditions (involving a step change in the reaction conditions and/or a change in solid and gas mass flow rates in the reactor) and (ii) operation mode in steady sate.

An example of dynamic conditions in the reactor is the first reaction step where the bed is initially partially filled with dehydrated solids from previous tests or with fresh CaO (around 3 kg). During the first few minutes when no solids are being fed in (see Figure 3 from 0 to 50 min) and in suitable reaction conditions, the bed of solids behaves as a

batch reactor. Gradually the conversion of the solids changes with time until the complete reaction of the solids in the bed is achieved (see min 15 in Figure 3). The modeling for this "batch stage" was recently formulated for a different batch fluidized bed facility [32] but with similar geometric characteristics to the facility described in this study. The mass balance applied to the $H_2O_{(v)}$ in a control volume of the complete reactor can be written as follows:

$$F_{H2O,Hy\,in} - F_{H2O,Hy\,exit} = N_{Ca\,active} \cdot r_{Hy,e} \quad (1)$$

The $r_{Hy,e}$ term is characteristic of the intrinsic reaction kinetics of the CaO material (in the emulsion phase), which is assumed to follow a shrinking core model[16]:

$$r_{Hy,e} = k_{Hy}^{2/3} \left(v_{H2O,e} - v_{H2O,eq}\right)\left(1 - X_{Hy}\right) \quad (2)$$

where k_{Hy} is the effective kinetic constant of the material reacting in the emulsion phase and $v_{H2O,\,e}$ and $v_{H2O,\,eq}$ the fractions of $H_2O_{(v)}$ in the emulsion phase and at equilibrium conditions[36] respectively. The gas exchange between the bubble and emulsion phases required for the calculation of $v_{H2O,\,e}$ is characterized using the same cross-flow factor (X_{factor}=1.5) as in a previous work[32]. From the mass balance applied to the water vapour in the bubble phase, the fraction of $H_2O_{(v)}$ in the bubble and emulsion phases can be related by the following equation (3):

$$v_{H2O,\,b,exit} = v_{H2O,e} + \left(v_{H2O,\,b,in} - v_{H2O,e}\right) \exp\left(-X_{factor}\right) \quad (3)$$

where at the exit:

$$v_{H2O,exit} = v_{H2O,e} \cdot \left(u_{mf}/u\right) + v_{H2O,b,\,exit} \cdot \left(\left(u - u_{mf}\right)/u\right) \quad (4)$$

$$F_{H2O,Hy\,exit} = \left(F_{air} \cdot v_{H2O,exit}\right)/\left(1 - v_{H2O,exit}\right) \quad (5)$$

Finally, the change in solids conversion over time is solved for small increments of time by means of the following general mass balance:

$$X_{Hy,t+\Delta t} = X_{Hy,t} + \frac{\left(F_{H2O,Hy\ in} - F_{H2O,Hy\ exit}\right)}{N_{Ca\ active}}(t+\Delta t) \qquad (6)$$

The previous equations (1-6) are solved for each time t to find, by means of a solver tool, the value of X_{Hy} that makes the $F_{H2O,Hy\ exit}$ and $v_{H2O,\ e}$ values meet in the previous mass balances of the gas and solid phases. The initial parameters that need to be taken into account to solve the model are: the moles of active CaO in the bed ($N_{Ca\ active}$), the inlet molar flows of $H_2O_{(v)}$ and air ($F_{H2O,in}$ and F_{air} respectively), the bed temperature (T_{Bed}, assumed to be constant) and the kinetic parameters. The kinetics of the CaO material used in this work (commercial "overburned" lime material supplied by Carmeuse, 200-800 μm, obtained from the calcination of $CaCO_3$ at around 1000ºC) has been characterized elsewhere[32]. The material showed incomplete conversion of CaO to $Ca(OH)_2$ due to its limited porosity resulting from the severe calcination conditions. For most samples, a fraction of inert material (i.e. molar fraction of non-reactive CaO) of $f_{inert}\approx 0.6$ was measured. Figure 7 shows the experimental mass flow of $H_2O_{(v)}$ (dots and smooth line, denoted by "Experimental*") and the prediction given by the model for the batch mode operation of the experiment in Figure 3. As can be seen, the batch reactor model is able to predict the new experimental results reasonably well when using the same $X_{factor}=1.5$ fitted previously for a different reactor[32]. The X_{factor} value is within the range of values expected in other bubbling reactors[25, 37].

For the hydration and dehydration tests with the continuous infeed of solids to the reactor, we also used the Kunii-Levenspiel model as described elsewhere[24] to discuss certain energy storage process concepts.

Consistent with the previous equation (1), the mass balance between the gases and solids in the reactor is:

$$F_{H2O,\,Hy\,in} - F_{H2O,\,Hy\,exit} = F_{Ca} \cdot \left(\bar{X}_{Hy} - \bar{X}_{Dehy}\right) \qquad (7)$$

where $\bar{X}_{Dehy}$ is the initial dehydration conversion of the solids introduced into the bed, $\bar{X}_{Hy}$ is the average hydration conversion of the solids in the reactor, calculated as the average of the individual hydration conversion of particles for a given residence time in the bed (it being assumed to be perfectly and instantly mixed):

$$\bar{X}_{Hy} = \int_0^{\infty} \left(X(t)\right) \cdot \left(\left(1/\tau\right) \exp\left(-t/\tau\right)\right) \cdot dt \qquad (8)$$

where τ is the average particle residence time in the reactor (N_{Ca}/F_{Ca}).

Concerning the kinetics of the particles in the reactor (as a function of their conversion and therefore of their residence time), the kinetic equation (2) for each individual particle can be integrated to obtain equation (9), where the solids conversion (with respect to the non-inert fraction of the solids infeed) is formulated as a function of their residence time as follows:

$$\begin{cases} X_{Hy}(t) = 1 - \left(1 - t\,k_{Hy}\right)^3 & \text{for } t < t^* \\ X_{Hy} = 1 & \text{for } t \geq t^* \end{cases} \qquad (9)$$

where t* is the time required to achieve maximum conversion, according to the shrinking core model, for a certain temperature and fraction of water vapor in the emulsion (still unknown until the mass balance in the gas phase has been solved). The concepts of t* and f_a are also linked to the assumption of a perfect mixing of solids in the bed:

$$f_a = \int_0^{t^*} \left(1/\tau\right) \exp\left(-t/\tau\right) dt \qquad (10)$$

where the time required to achieve the maximum conversion (t*) can be obtained by integrating equation (10) as follows:

$$t^* = -\tau \cdot Ln(1 - f_a) \qquad (11)$$

Since the moles of $Ca(OH)_2$ that appear in the bed during hydration must match the moles of Ca reacting in the bed, the general mass balance applied to the reactor can be written as:

$$F_{Ca} \cdot \left(\bar{X}_{Hy} - \bar{X}_{Dehy}\right) = N_{Ca\ active} \cdot f_a \cdot r_{Hy,e} \qquad (12)$$

By combining equations (2) and (12), the average conversion can be written as:

$$\bar{X}_{Hy} = 1 - \left(1 - \frac{F_{Ca} \cdot \left(X_{Hy} - \bar{X}_{Dehy}\right)}{\left(v_{H2O,\,e} - v_{H2O,\,eq}\right) N_{Ca\ active} \cdot f_a \cdot 3k_{Hy}}\right)^{3/2} \qquad (13)$$

At this point, the model can be solved (for example by means of the solver tool of Excel) by iterating the fraction of active particles of CaO in the bed, f_a, so that the solids conversion in the emulsion phase calculated from equation (13) is the same as that of equation (8). For those tests where $v_{H2O,in}<1$, the fractions of $H_2O_{(v)}$ in the emulsion and bubble phases are related by equations (3-5) using the X_{factor} parameter.

The predictions given by the previous reactor model, have been compared to assist in the interpretation of the results obtained in this new facility for a given solids input molar flow (F_{Ca}) with a certain inert content (f_{inert}) using as input data for the model the molar flows of the input gases ($F_{H2O,\,in}$ and F_{air}), the bed temperature (T_{Bed}, assumed to

be constant during the testing), the total inventory of calcium (N_{Ca}) and the kinetic information at particle level of the Ca material measured independently[32].

Figure 8 shows the experimental and model-predicted curves for different hydration and dehydration tests operating in continuous mode. A reasonable quality match can be observed between the experimental results and model predictions, considering that no fitting parameters have been introduced into the model calculations (the same X_{factor}=1.5, as in the previous work on batch reactor data[32] has been applied together with the same kinetics parameters for CaO hydration and dehydration independently obtained by thermogravimetric tests). For the sake of simplicity, the results provided in Figure 8 are plotted for times that extend from the starting point of the solids infeed to $t=2\cdot\tau$, where τ is between 2000 and 2300 s once the steady state has been reached (equivalent to solids inventories of between 650 and 900 kg/m^2), but they extend for more than 4-5 hours in steady state, as explained in the Experimental section. The good agreement between the experimental and model-predicted $m_{H2O,\ exit}$ is further highlighted in Figure 9 for several experimental series, by comparing the experimental $m_{H2O,\ exit}$ (after smoothing out the experimental signal to reduce noise) with the predictions made by the model in one plot.

Future testing campaigns, will consider higher solid flow rates or operation conditions closer to equilibrium (i.e. hydration at higher temperatures or dehydration under fraction of $H_2O_{(v)}$ higher than 0) in order to evaluate the effect of lower reaction rates and higher steam consumption/generation on the hydration/dehydration reactions in the bed. This will allow us to further progress on the evaluation of these reactors for the scaling up of the results and models developed in this study for future large scale $CaO/Ca(OH)_2$ energy storage systems.

Conclusions

Proof of the viability of the $CaO/Ca(OH)_2$ hydration/dehydration chemical loop for thermochemical energy storage using fluidized bed reactors has been obtained in a 20 kW continuous pilot plant. The fluidized bed reactor has been successfully operated under hydration and dehydration conditions at high fluidization velocities (around 0.6 m/s), temperatures between 400-540ºC, $H_2O_{(v)}$ fractions from 0 to 1 and the continuous feeding and extracting of around 10-13 kg/s of commercial CaO. During the hydration mode, it is possible to obtain consistent values of solid and gas conversion from experimental measurements of the water vapor content in the gas phase and by applying a heat balance to the reactor. During the dehydration reaction only the change in gas concentration can be used to follow the dehydration conversion. Using experimental information from both the steady state and the dynamic part of the experiments, it is possible to fit the results obtained to a standard KL bubbling reactor model using a cross flow factor parameter consistent with previous works and kinetic information specific to the material used during the pilot experiments. The model developed predicts reasonably well the modes of reactor operation observed during the experiments under dynamic conditions (after a step change in the reaction conditions and/or a change in the solid and gas mass flow rates in the reactor) and operation modes in steady sate. Although more experimental studies in this new facility are required, this work provides a preliminary set of validated results for the future scaling up of thermochemical energy storage technology using fluidized beds.

Acknowledgements

Financial support provided by the European Commission under the 7th Framework Program (StoRRe Project GA 282677) is acknowledged. Y.A. Criado thanks the Government of the Principality of Asturias for a Ph.D. fellowship (Severo Ochoa Program).

Nomenclature

f_a fraction of active (non-reacted) Ca material in the reactor

F_i molar flow of component i, mol/s

f_{inert} molar fraction of inert material present in the solids

k kinetic constant, s^{-1}

m_i mass flow of component i, kg/h

N_{Ca} moles of total Ca present in the bed, mol

$N_{Ca\ active}$ moles of active Ca material present in the bed (non-inert), mol

r_i reaction rate, s^{-1}

t reaction time, s

t* time required to achieve the maximum conversion, s

T_{Bed} bed temperature, ºC

u input gas velocity, m/s

u_{mf} velocity at minimum fluidization conditions, m/s

X conversion of active material, mol H_2O/mol CaO active

$\bar{X}$ average conversion

X_{factor} cross flow factor

Greek symbols

τ average particle residence time, s

ν_{H2O} fraction of $H_2O_{(v)}$

$\nu_{H2O,eq}$ equilibrium fraction of $H_2O_{(v)}$

Subscripts

b bubbles

Dehy dehydration reaction

e emulsion

Hy hydration reaction

in input conditions

exit exit conditions

H_2O water vapour

air inert gas (i.e. air)

Ca Ca-based solids

References

(1) IPCC Climate change 2014: Synthesis report. Contribution of Working Group I, II and III to the Fifth Assessment Report of the Intergovernmental Panel on Climate Change; International Panel on Climate Change: Geneva, Switzerland, 2014; p 151.

(2) IEA World energy outlook special report: Energy and climate change; International Energy Agency: Paris, France, 2015.

(3) IRENA Renewable capacity statistics 2016; International Renewable Energy Agency: United Arab Emirates, 2016.

(4) IEA Technology roadmap: Energy storage; International Energy Agency: Paris, France, 2014.

(5) Prieto, C.; Cooper, P.; Fernández, A. I.; Cabeza, L. F. Review of technology: Thermochemical energy storage for concentrated solar power plants. *Renew. Sust. Energ. Rev.* **2016,** *60*, 909.

(6) Zhang, H.; Baeyens, J.; Cáceres, G.; Degrève, J.; Lv, Y. Thermal energy storage: Recent developments and practical aspects. *Prog. Energ. Combust.* **2016,** *53*, 1.

(7) Kuravi, S.; Trahan, J.; Goswami, D. Y.; Rahman, M. M.; Stefanakos, E. K. Thermal energy storage technologies and systems for concentrating solar power plants. *Prog. Energ. Combust.* **2013,** *39*, 285.

(8) Pardo, P.; Deydier, A.; Anxionnaz-Minvielle, Z.; Rougé, S.; Cabassud, M.; Cognet, P. A review on high temperature thermochemical heat energy storage. *Renew. Sust. Energ. Rev.* **2014,** *32*, 591.

(9) Cot-Gores, J.; Castell, A.; Cabeza, L. F. Thermochemical energy storage and conversion: A-state-of-the-art review of the experimental research under practical conditions. *Renew. Sust. Energ. Rev.* **2012,** *16*, 5207.

(10) Felderhoff, M.; Urbanczyk, R.; Peil, S. Thermochemical Heat Storage for High Temperature Applications – A Review. *Green* **2013,** *3*, 113.

(11) André, L.; Abanades, S.; Flamant, G. Screening of thermochemical systems based on solid-gas reversible reactions for high temperature solar thermal energy storage. *Renew. Sust. Energ. Rev.* **2016,** *64*, 703.

(12) Aydin, D.; Casey, S. P.; Riffat, S. The latest advancements on thermochemical heat storage systems. *Renew. Sust. Energ. Rev.* **2015,** *41*, 356.

(13) Ervin, G. Method of storing and releasing thermal energy. U.S. Patent No. 3.973.552, 1976.

(14) Bauerle, G. L.; Chung, D.; Ervin, G.; Guon, J.; Springer, T. H. In *Storage of solar energy by inorganic oxide/hydroxides*, Proceedings of Sharing the Sun: Solar technology in the seventies, Winnipeg, Canada, 1976; International Solar Energy Society of Canada: 8.

(15) Ervin, G. Solar heat storage using chemical reactions. *J. Solid State Chem.* **1977,** *22*, 51.

(16) Criado, Y. A.; Alonso, M.; Abanades, J. C. Kinetics of the $CaO/Ca(OH)_2$ hydration/dehydration reaction for thermochemical energy storage applications. *Ind. Eng. Chem. Res.* **2014,** *53*, 12594.

(17) Edwards, S. E. B.; Materić, V. Calcium looping in solar power generation plants. *Sol. Energy* **2012,** *86*, 2494.

(18) Chacartegui, R.; Alovisio, A.; Ortiz, C.; Valverde, J. M.; Verda, V.; Becerra, J. A. Thermochemical energy storage of concentrated solar power by integration of the calcium looping process and a CO_2 power cycle. *Appl. Energ.* **2016,** *173*, 589.

(19) Frazer, D.; Stergar, E.; Cionea, C.; Hosemann, P. Liquid metal as a heat transport fluid for thermal solar power applications. *Energy Procedia* **2014,** *49*, 627.

(20) Ho, C. K.; Iverson, B. D. Review of high-temperature central receiver designs for concentrating solar power. *Renew. Sust. Energ. Rev.* **2014,** *29*, 835.

(21) Flamant, G.; Olalde, G. High temperature solar gas heating comparison between packed and fluidized bed receivers—I. *Sol. Energy* **1983,** *31*, 463.

(22) Flamant, G.; Hemati, M. Device for collecting solar energy. U.S. Patent Appl. 2013/0284163 A1 2013.

(23) Boissiere, B.; Ansart, R.; Gauthier, D.; Flamant, G.; Hemati, M. Experimental hydrodynamic study of gas-particle dense suspension upward flow for application as new heat transfer and storage fluid. *Can. J. Chem. Eng.* **2015,** *93*, 317.

(24) Criado, Y. A.; Alonso, M.; Abanades, J. C.; Anxionnaz-Minvielle, Z. Conceptual process design of a $CaO/Ca(OH)_2$ thermochemical energy storage system using fluidized bed reactors. *Appl. Therm. Eng.* **2014,** *73*, 1089.

(25) Kunii, D.; Levenspiel, O. *Fluidization Engineering*; 2nd ed.; Butterworth-Heinemann: USA, 1991.

(26) Yan, J.; Zhao, C. Y. Experimental study of $CaO/Ca(OH)_2$ in a fixed-bed reactor for thermochemical heat storage. *Appl. Energ.* **2016,** *175*, 277.

(27) Schaube, F.; Kohzer, A.; Schütz, J.; Wörner, A.; Müller-Steinhagen, H. De- and rehydration of $Ca(OH)_2$ in a reactor with direct heat transfer for thermo-chemical heat storage. Part A: Experimental results. *Chem. Eng. Res. Des.* **2013,** *91*, 856.

(28) Schmidt, M.; Szczukowski, C.; Roßkopf, C.; Linder, M.; Wörner, A. Experimental results of a 10 kW high temperature thermochemical storage reactor based on calcium hydroxide. *Appl. Therm. Eng.* **2014,** *62*, 553.

(29) Schaube, F.; Utz, I.; Wörner, A.; Müller-Steinhagen, H. De- and rehydration of $Ca(OH)_2$ in a reactor with direct heat transfer for thermo-chemical heat storage. Part B: Validation of model. *Chem. Eng. Res. Des.* **2013,** *91*, 865.

(30) Fujii, I.; Tsuchiya, K.; Higano, M.; Yamada, J. Studies of an energy storage system

by use of the reversible chemical reaction: $CaO + H_2O \rightleftharpoons Ca(OH)_2$. *Sol. Energy* **1985,**

34, 367.

(31) Kanzawa, A.; Arai, Y. Thermal energy storage by the chemical reaction augmentation of heat transfer and thermal decomposition in the $CaO/Ca(OH)_2$ powder. *Sol. Energy* **1981,** *27*, 289.

(32) Criado, Y. A.; Huille, A.; Rougé, S.; Abanades, J. C. Experimental investigation and model validation of a $CaO/Ca(OH)_2$ fluidized bed reactor for thermochemical energy storage applications. *Chem. Eng. J.* **2016**, http://dx.doi.org/10.1016/j.cej.2016.11.010.

(33) Pardo, P.; Anxionnaz-Minvielle, Z.; Rougé, S.; Cognet, P.; Cabassud, M. $Ca(OH)_2/CaO$ reversible reaction in a fluidized bed reactor for thermochemical heat storage. *Sol. Energy* **2014,** *107*, 605.

(34) Criado, Y. A.; Alonso, M.; Abanades, J. C. Composite material for thermochemical energy storage using $CaO/Ca(OH)_2$. *Ind. Eng. Chem. Res.* **2015,** *54*, 9314.

(35) Criado, Y. A.; Alonso, M.; Abanades, J. C. Enhancement of a $CaO/Ca(OH)_2$ based material for thermochemical energy storage. *Sol. Energy* **2016,** *135*, 800.

(36) Barin, I. *Thermochemical data of pure substances*; VCH Verlagsgesellschaft Weinheim, Germany, 1989.

(37) Davidson, J. F.; Harrison, D. P. *Fluidized Particles*; Cambridge University Press: New York, 1963.

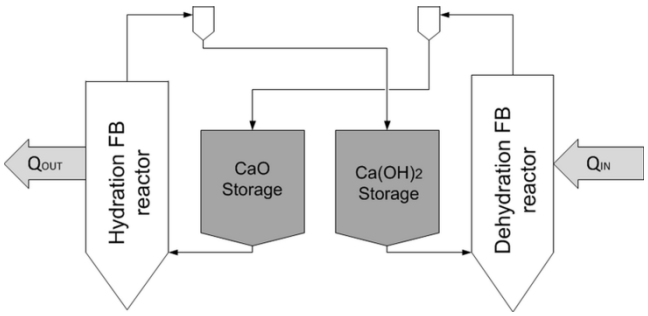

Figure 1. Basic conceptual scheme of the $CaO/Ca(OH)_2$ energy storage system

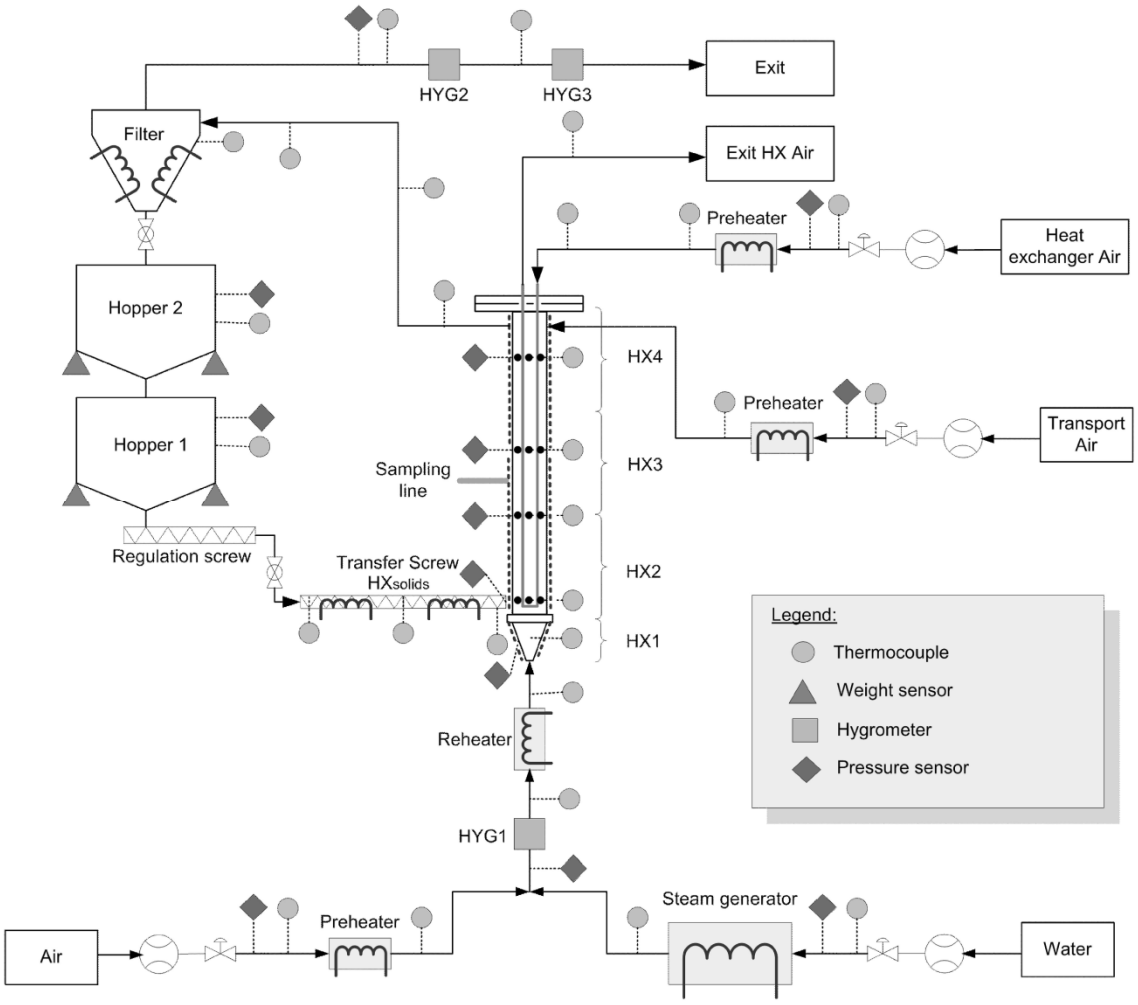

Figure 2. Schematic view of the continuous fluidized bed pilot plant at CEA-Grenoble for investigating the hydration/dehydration reaction of $CaO/Ca(OH)_2$

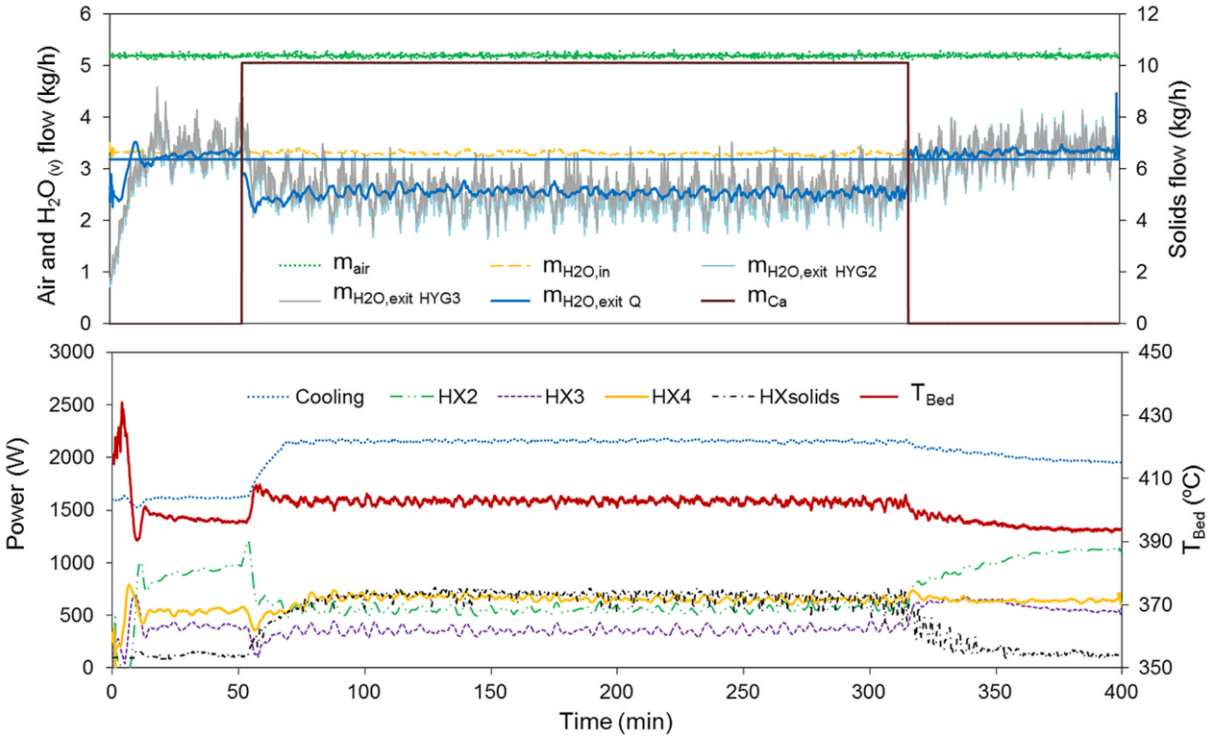

Figure 3. Main signals measured vs. time in a typical hydration test. Notice that the "Cooling" thermal power is removed from the bed, while the HX2- 4 and solids thermal power is supplied by the electric wires to the bed.

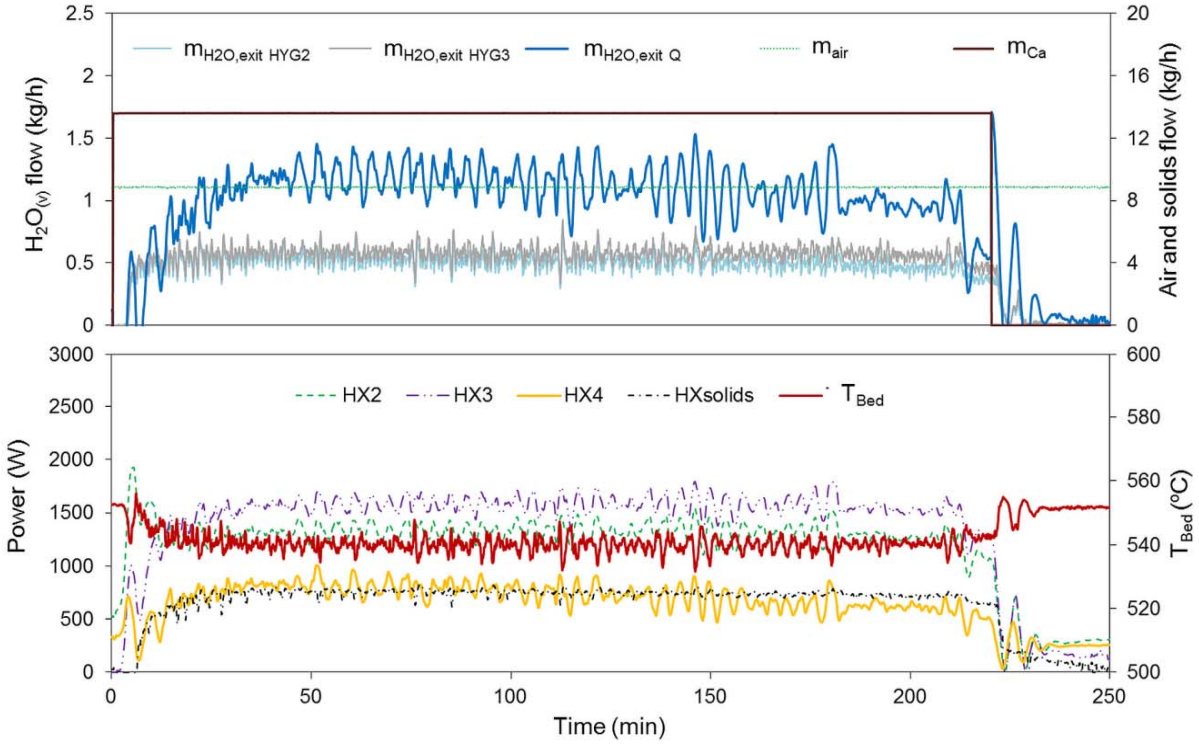

Figure 4. Main signals measured vs. time in a typical dehydration test.

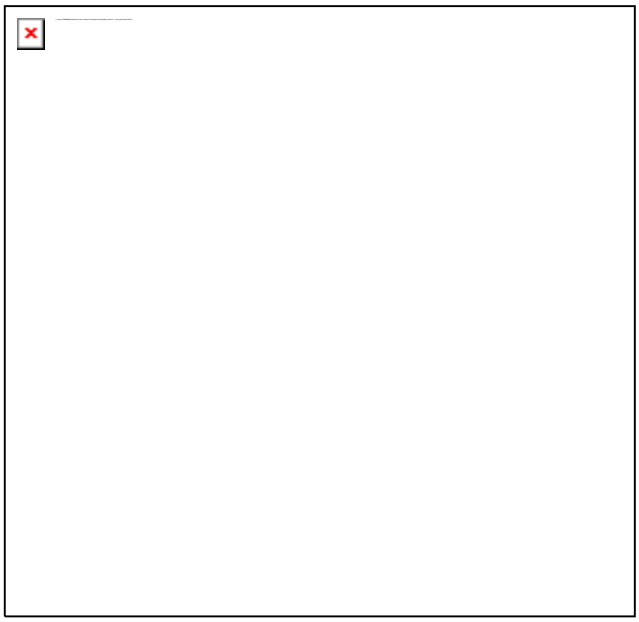

Figure 5. Comparison of the mass flow of steam during hydration at the exit of the reactor ($m_{H2O,exit\ Hy}$) measured by the hygrometers and by the heat balance for different hydration tests.

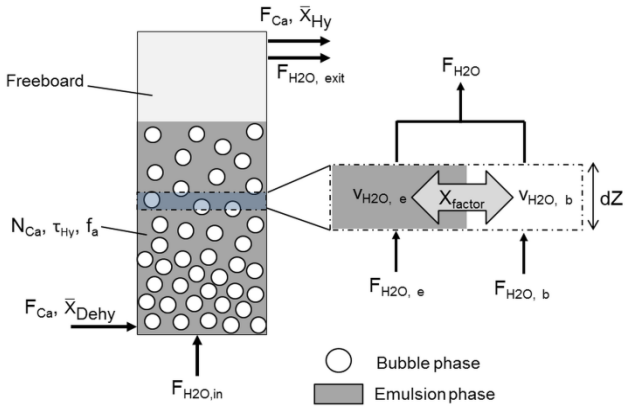

Figure 6. Schematic representation of the bed reactor during the hydration operation in continuous mode, labeled using the notation employed for the main variables in the continuous reactor model.

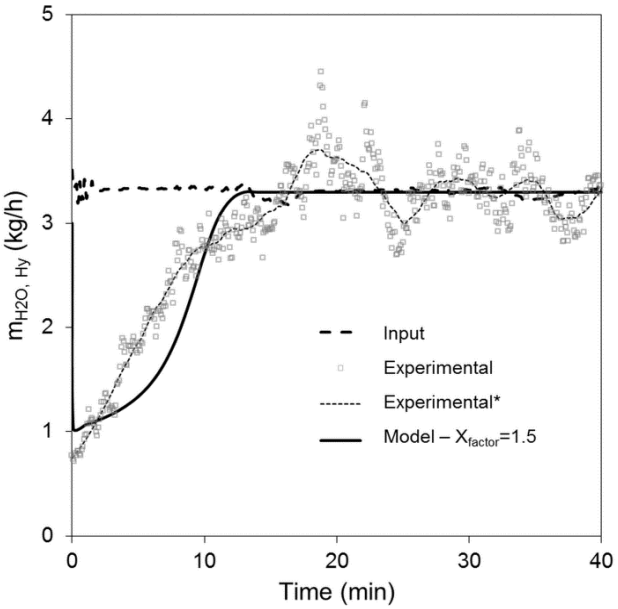

Figure 7. Experimental and model-predicted mass flow of $H_2O_{(v)}$ during the batch operation mode in the hydration test shown in Figure 3. The input molar flow of $H_2O_{(v)}$ is represented as dotted lines for reference. The "Experimental*" smooth curve was obtained by using a Savitzky-Golay smooth 4rd degree filter.

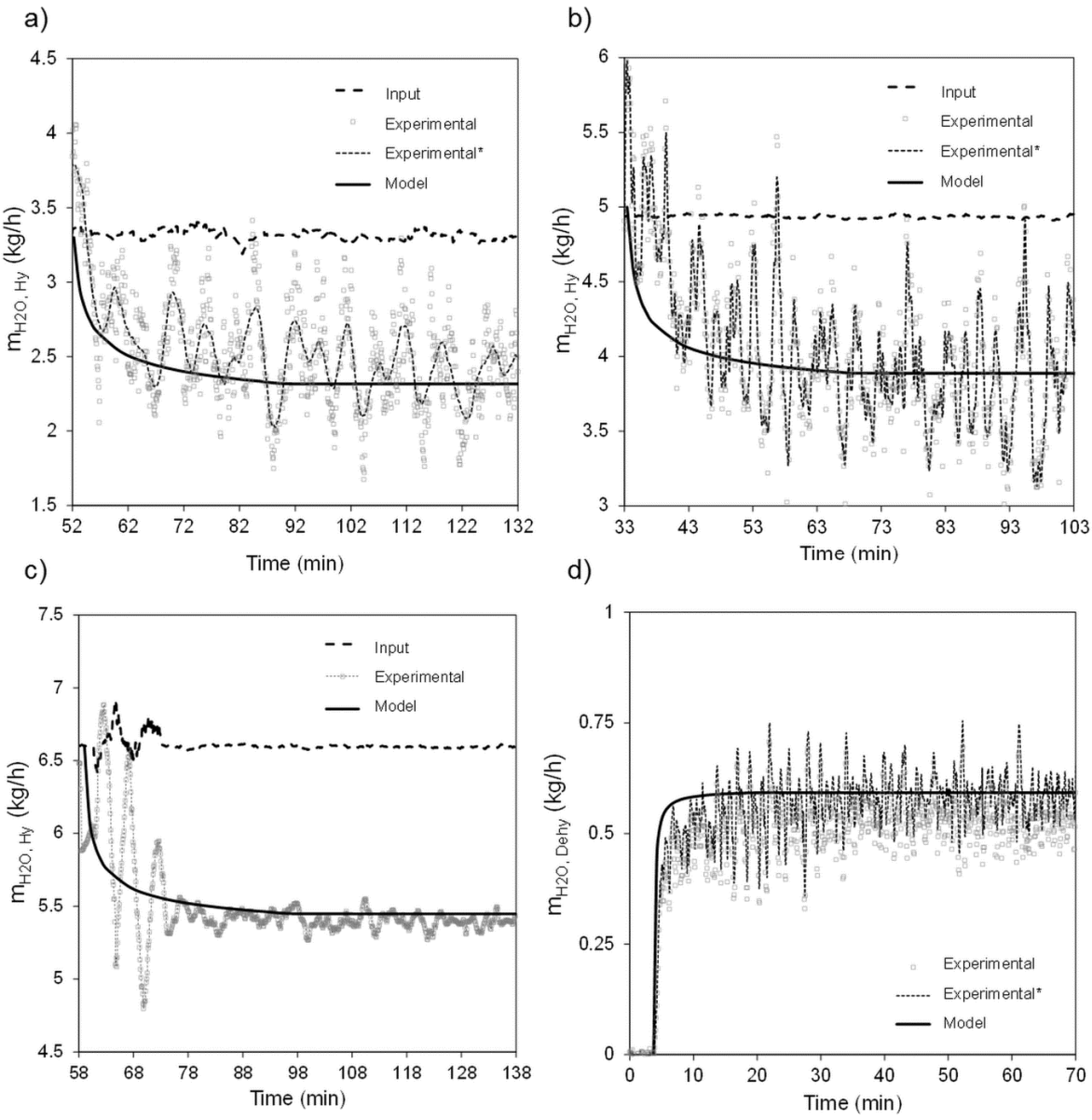

Figure 8. Experimental and model-predicted mass flow of $H_2O_{(v)}$ during the continuous operation mode for **a-c)** hydration tests at 400ºC , $\nu_{H2O,in\ Hy}$ of 0.5, 0.75 and 1 and m_{Ca} of 10.1, 11.6 and 10.2 kg/h respectively and **d)** dehydration test at 540ºC, $\nu_{H2O,in\ Dehy}$=0 and m_{Ca}=13.6 kg/h. The input molar flow of $H_2O_{(v)}$ is represented as dotted lines for reference. For the sake of simplicity the m_{H2O} values are only reported for the time between the starting point of the solids infeed and t=2·τ. "Experimental*" smooth curve as above.

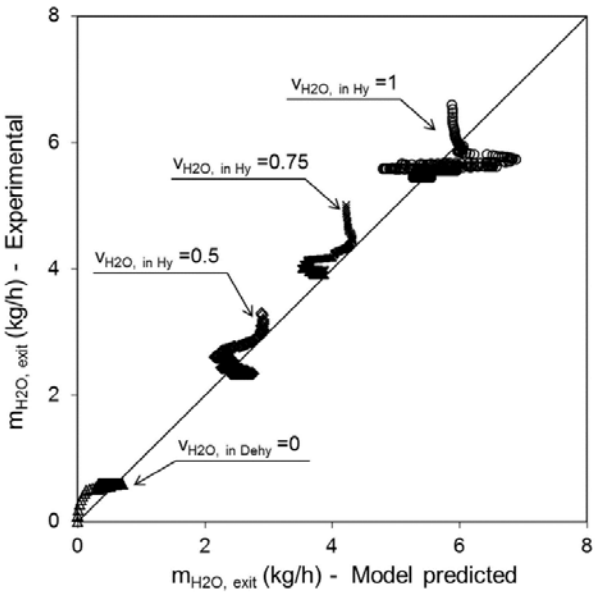

Figure 9. Comparison of the experimental and predicted mass flow of $H_2O_{(v)}$ at the reactor exit during the continuous operation mode for the first experimental vs. model results shown in Figure 8. For simplicity the $m_{H2O,\ exit}$ values are only reported for times between the starting point of the solids infeed and $t=2\cdot\tau$.

For Table of Contents Only